Graphene Oxide Mixed Matrix Membranes for Improved Desalination Performance

by

Adam A. Inurria

A Thesis Presented in Partial Fulfillment
of the Requirements for the Degree
Master of Science

Approved April 2017 by the
Graduate Supervisory Committee:

Francois Perreault, Co-Chair
Peter Fox, Co-Chair
Mary Laura Lind

ARIZONA STATE UNIVERSITY

May 2017

ABSTRACT

Reverse osmosis (RO) membranes are considered the most effective treatment to remove salt from water. Specifically, thin film composite (TFC) membranes are considered the gold standard for RO. Despite TFC membranes good performance, there are drawbacks to consider including: permeability-selectivity tradeoff, chlorine damage, and biofouling potential. In order to counter these drawbacks, polyamide matrixes were embedded with various nanomaterials called mixed matrix membranes (MMMs) or thin film nanocomposites (TFNs). This research investigates the use of graphene oxide (GO) and reduced graphene oxide (RGO) into the polyamide matrix of a TFC membrane. GO and RGO have the potential to alter the permeability-selectivity trade off by offering nanochannels for water molecules to sieve through, protect polyamide from trace amounts of chlorine, as well as increase the hydrophilicity of the membrane thereby reducing biofouling potential. This project focuses on the impacts of GO on the permeability selectivity tradeoff. The hypothesis of this work is that the permeability and selectivity of GO can be tuned by controlling the oxidation level of the material. To test this hypothesis, a range of GO materials were produced in the lab using different graphite oxidation methods. The synthesized GOs were characterized by X-ray diffraction and X-ray photoelectron microscopy to show that the spacing is a function of the GO oxygen content. From these materials, two were selected due to their optimal sheet spacing between 3.4 and 7 angstroms and embedded into desalination MMM. This work reveals that the water permeability coefficient of MMM embedded with GO and RGO increased significantly; however, that the salt permeability coefficient of the membrane also increased. Future research directions are proposed to overcome this limitation.

ACKNOWLEDGMENTS

This paper is in honor of the incredible, loving family that has supported me along my journey of sciences and engineering. My father who pushes me, my mother who supports me, and my brother who questions me. Without each force in my life, I would not be the man that I am today.

Furthermore, I would like to thank my advisor Dr. Francois Perreault for his determination in the field of science and dedication to his students' success. He truly has enlightened my scientific understanding, heightened my expectations for a scientific outlook, as well as broadened my perspective of relationships with peers, mentors, and up-and-coming prospects more than I could have thought imaginable. I wish you the best in your future endeavors as I know you will succeed.

To the fellow students I met along the way, I thank you for your support and the close moments we shared. I loved our cohort of engineering students and I couldn't have imagined it any other way.

To NSF for supporting NEWT research purposes in determination of finding real world applications for nanotechnology in water treatment operations.

To ASU faculty for investing their time and resources to address these real world solutions and attracting fellow, bright-minded professionals along the way. I wish the best for your community as well as the motivated folks that are drawn to your responsible outlook to our environment.

TABLE OF CONTENTS

Page

LIST OF TABLES……..…….v

LIST OF FIGURES…...……..vi

CHAPTER

1 INTRODUCTION……...….1

1.1 Overview…….....1

1.2 Statement of Purpose…….……..4

1.3 Hypothesis and objectives ……5

2 BACKGROUND LITERATURE……6

2.1 Membranes Processes for Water Treatment……..……..….6

2.2 Desalination by Membrane-Based Reverse Osmosis Membranes……...9

2.3 Graphene Oxide Novelty and Desalination Potential……..11

2.4 Nanomaterial-based Mixed Matrix Membranes for Desalination …..……13

3 METHODOLOGY ……17

3.1 Graphene Oxide Synthesis …….....17

3.1.1 Staudenmaier Synthesis……...……..17

3.1.2 Hofmann Synthesis……18

3.1.3 Tour Synthesis……...……18

3.1.4 Tung Synthesis……...……...19

3.1.5 Mercapto Reduced GO Synthesis……..20

3.2 Graphene Oxide Characterization ……..……21

3.3 TFC and TFC embedded with GO and MRGO Membrane Casting ……...23

CHAPTER Page

3.4 Casted MMM and TFC RO Performance Testing……..25

4 RESULTS AND DISCUSSION ……..……...….28

4.1 Graphene Oxide Characterization……...28

4.2 Material Selection for Membrane Fabrication……...….31

4.3 Morphological Characterization of GO……..32

4.4 Morphological Characterization of GO, MRGO, and TFC Membranes….34

4.5 GO, MRGO, and TFC Membrane RO Performance …...……...34

5 CONCLUSION……..……...…….……36

REFERENCES……..…… 38

APPENDIX

A EQUATIONS……...…..…….....44

LIST OF TABLES

Table Page

4. 1 Corresponding Graphene Sheet Spacing, 2θ Values, and Carbon to Oxygen Ratios for each GO 29

4. 2 Raman Spectroscopy of D to G Intensity Ratio for Graphite, Staudenmaier GO, Tour GO, and Tung GO..... 31

LIST OF FIGURES

Figure Page

1. 1 Bonding Structure of Meta-Phenylenediamine, Trimesoyl Chloride, and Polyamide 3

2. 1 Illustration of Membrane Types and the Size and Type of Contaminants Removed by Each..... 7

2. 2 Schematic Image of GO Molecular Structure..... 12

2. 3 Oxidation of Graphite Using Different Protocols..... 13

2. 4 Illustration of MMM with GO Embedded in the Thin-Film Layer of Crosslinked-Polyamide.. 15

2. 5 Illustration of the Changes in GO (gray) in Molecular strucutre from (a) Room Temperature, (b) 100ºC, (c) 220ºC, and (d) 500ºC. The Yellow Color is Unoccupied Lattice Space. 16

3. 1 Illustration of the Formation of Polyamide with and without GO. MPD in Red, TMC in Yellow, GO Dispersed in TMC in Black and Yellow, Polyamide in Brown..... 23

4. 1 XRD Graphs for Graphite and all GO Synthesises..... 28

4. 2 C:O Ratio as a Function of Interlayer Spacing for GO, MRGO, and Graphite..... 29

4. 3 Raman Spectroscopy for Staudenmaier, Tour and Tung Graphene Oxides as well as the Starting Graphite. 30

4. 4 SEM of MRGO. 32

4. 5 SEM Images of Staudenmaier GO..... 32

4. 6 (a) AFM and (b) Thickness Analysis of MRGO. 33

4. 7 AFM Image of Staudenmaier GO. 33

4. 8 From Left to Right, SEM images of TFC, STGO-MMM, and MRGO-MMM..... 34

Figure 4. 9:Average water and salt permeability coefficients for 3 membranes: TFC, TFN-STGO, and TFN-MRGO. 35

CHAPTER 1

INTRODUCTION

1.1 Overview

Reverse osmosis (RO) thin-film composite (TFC) membrane technologies are the most advanced treatment design for removing salts from water. They offer lower energy requirements than thermal technologies (Semiat 2008). The removal of salts occurs because the active polyamide layer is impermeable and requires significant pressure loading to force water passage through the membrane. Water solubilizes in the polyamide and diffuses through the active layer without salt (Paul 2004). However, a small fraction of salt manages to maintain solubility within the water thus accounting for the imperfect rejection. The state of the art in desalination RO membranes achieves an effluent with 99.85% salt removal at an energy efficiency of 1.8 kWh/m^3 (Elimelech and Philip 2011).

Despite TFC membranes leading in the field of desalination, these technologies are limited by the permeability-selectivity tradeoff, significant energy demand, their vulnerability to chlorine damaging, and their biofouling potential (Misdan, Lau and Ismail 2011) (Geise, et al. 2011). RO membranes experience a significant drawback in permeability due to their high selectivity. RO requires a significant pressure to operate thus requiring high energy demand, albeit not as high as thermal processes. Additionally, due to the need for high removal of salts and imperfect rejection of RO membranes, multiple RO passes are required to improve effluent quality, increasing operation cost (Werber, Deshmukh and Elimelech, 2016).

Membrane development incorporating nanomaterials into the membrane structure has been highlighted as a strategy to address these limitations of TFC membranes (Qu, Alvarez and Li 2013) (Tiraferri, et al. 2012) (Pendergast and Hoek 2011). The surface energy of membranes can be tuned by addition of hydrophilic nanomaterials to reduce the deposition of foulants (Tiraferri, et al. 2012). Antimicrobial nanomaterials can be used to control the growth of microorganisms to reduce biofouling (Pendergast and Hoek 2011) (Perreault, Tousley and Elimelech, 2014) (Qu, Alvarez and Li 2013). Finally, the permselectivity of the membrane can be enhanced by incorporating nanoporous materials that can selectively let water molecules pass through.

Graphene-based membranes have attracted a lot of attention due to the exceptional transport rate of water in graphene nanochannels (Werber, Osuji and Elimelech, 2016). The atomic-level smoothness and hydrophobic properties of graphene allow water to flow virtually without friction (Joshi, et al. 2014). Graphene nanochannels for membrane separation have been attempted using carbon nanotubes, single-layer nanoporous graphene, and graphene laminated structures. Of these materials, graphene offers several advantages such as a lower cost and easier processing due to its two-dimensional structure (Mi 2014) (Perreault, de Faria and Elimelech 2015).

Previous research has investigated Pure GO membranes for their potential for desalination using GO deposited onto a sub-micron-pore filter (Amadei 2016). Research has determined that GO does reject salt, but not to the same extent as TFC (Sun 2016) (Amadei 2016) (Goh, et al. 2016) (Perreault 2015). Additionally, there is an adsorbent nature to GO that will initially remove salt until the material has utilized the entire area available or adsorption. After adsorption is no longer available for salt rejection, the pure

GO membrane will remove considerably less salt. Although pure GO membranes do not compete with the removal efficiency of TFC membranes, the ability for GO embedded in TFC to improve performance of the membrane should not be overlooked.

Two categories exist for implementing these nanomaterials 1) surface modification and 2) in-situ embedment into the polymer matrix. Both techniques demonstrate capabilities to counter the limitations for reverse osmosis. However, the surface modification approaches only affect surface properties, may lack scalability and do not offer good nanomaterial adhesion (Zodrow, et al. 2009) (Ismail, et al. 2009). These mixed matrix membranes (MMMs) offer a readily scalable approach to industry with added nanomaterial resiliency by being bound in a polyamide matrix (Mahmoud, et al. 2014).

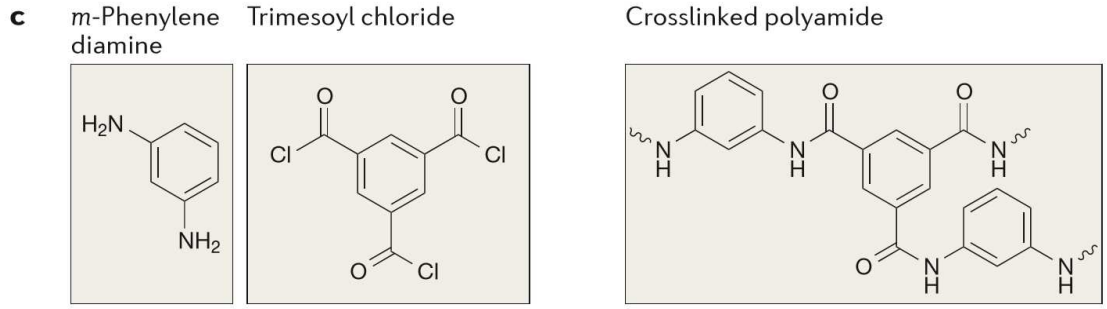

Figure 1. 1: Bonding Structure of meta-phenylenediamine and trimesoyl chloride, and polyamide (Werber, Osuji and Elimelech 2016).

For desalination membranes, embedding the nanomaterials in the thin polyamide film of the active layer allows them to contribute to permselectivity of the membrane. The active layer is formed by interfacial polymerization, a chemical reaction between two monomers m-phenylenediamine (MPD) and trimesoyl chloride (TMC) that form a non-porous, impermeable, crosslinked polyamide layer. Figure 1.1 illustrates the crosslinked nature resulting from interfacial polymerization. This bonding structure is necessary for high levels of selectivity in the TFC polyamide membranes (Elimelech and Philip 2011).

The highly crosslinked polyamide is responsible for the impermeable nature of the membrane and is the rate limiting step in water permeation through TFC membranes. Integrating nanomaterials into the active layers was found as a possible approach to overcome this limitation and thin film nanocomposite (TFN) membranes can offer higher performance than the traditional TFC membranes (Lind, et al. 2010) (Lind, et al. 2009) (Jeong, et al. 2007) (Ganesh, Isloor and Ismail 2013) (Ismail, et al. 2009).

Embedding GO into membranes in a MMM can be used to modify the transport of water across the membrane. Graphene laminates form nanochannels that can effectively separate from water from water solutes of dimension higher than the channel size (Mi 2014). This nanoscale sieving can be used to enhance desalination membranes if the channel dimensions can be tuned to subnanometer range to selectively let water molecules pass while rejecting salt ions. Achieving these pore sizes will allow the membrane to act as molecular sieves and transport water molecules through molecular size exclusion instead of the slower diffusion mechanism (Mi 2014). This change of separation mechanisms has the potential to improve permeability of the membrane without compromising its selectivity, thus breaking away from the permeability-selectivity trade-off of the current TFC technology.

1.2 Statement of Purpose

The purpose of this study is to evaluate the performance of MMMs embedded with GO and reduced GO and compare them to the gold standard TFC membranes for desalination applications. This work will investigate the effect of interlayer spacing and oxygen content on the water and salt permeability of graphene-based MMMs. The results

of this project will be useful to provide insight regarding the potential for innovative, scalable design of graphene-based MMMs for water treatment.

1.3 Hypothesis and Objectives

I hypothesize that the selectivity of MMM incorporating (GO) can be controlled by changing the oxygen content of GO sheets. According to this hypothesis, high performance GO-MMM desalination membranes will be achieved if GO sheets having an interlayer spacing in the desalination range of 3.4-7 angstroms are used (Werber, Osuji and Elimelech 2016) (Mi 2014). To evaluate this hypothesis, the following objectives will be pursued: (i) synthesize GO materials of different oxidation levels; (ii) characterize GO materials to establish a relationship between oxygen content and sheet spacing, (iii) embed GO sheets of selected sheet spacing in TFC membranes; (iv) evaluate the effect of GO on the permeability and selectivity of GO-MMMs.

CHAPTER 2

BACKGROUND LITERATURE

2.1 Membrane Processes for Water Treatment

In treatment processes, membranes are used to remove contaminants from water across a significant range of sizes and compositions. Furthermore, the use of various types of membranes exists to this day in regards to membrane composition and membrane pore size. Figure 1.1, adopted from Werber et al, illustrates a complete scale of membrane types with respect to the size and type of contaminants that are removed by each membrane (Werber, Osuji and Elimelech, Materials for next-generation desalination and water purification membranes 2016). Contaminants are important in determining proper membrane or filtration use, therefore, it is important to understand what pollutants –or micropollutants—are present in a given source water (Schwarzenbach 2006). Additionally, as water reuse applications become more widespread, the need for higher effluent quality from wastewater treatment facilities and their removal of a wide size range of contaminants will be necessary (Kolphin 2002) (Tang, et al. 2014). Overall, reverse osmosis is the necessary for the removal of 0.1-1nm, increasingly concerning contaminants.

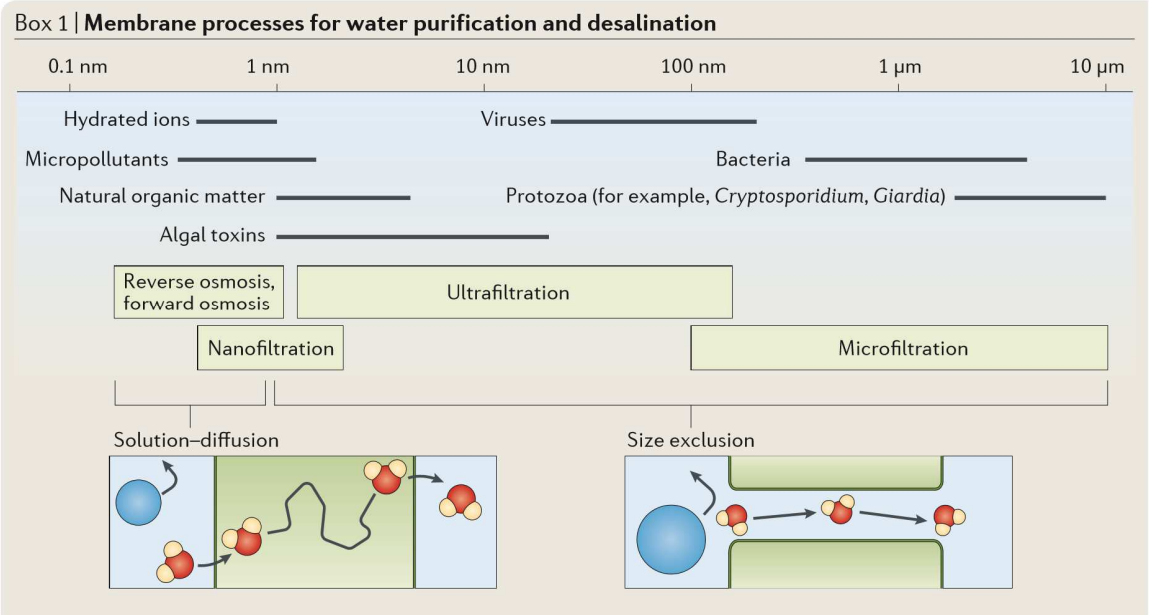

Figure 2. 1: Illustration of membrane types and the size and type of contaminants removed by each, adopted from J. Werber, 2016.

Membranes for water purification are utilized for their superior water quality, adaptability to feed quality oscillations, and require a much smaller footprint compared to older treatment designs (Shannon 2008). With the difficulty of treating nanometer sized contaminants in water, so much rise the complexation of treatment trains and technologies (M. Elimelech 2006).

These complex solutions inspired research for membranes of different base materials including: polymeric, cellulose, or inorganic (Werber, Osuji and Elimelech, 2016). Polymeric membranes are the most common due to their relatively low cost and ease of fabrication. Fabrication methods for producing polymeric membranes are: phase inversion membranes, track etching, and thin film composite (TFC) membranes.

Phase inversion membranes make up the majority of microfiltration and ultrafiltration porous, polymer membranes. The method requires the precipitation of a dissolved polymer in a thin film to produce a porous membrane structure (Werber, Osuji

and Elimelech, 2016) (Baker 2012). The technique used for phase inversion is called non-solvent induced phase separation (NIPS) (Werber, Osuji and Elimelech, Materials for next-generation desalination and water purification membranes 2016). NIPS has a film of dissolved polymer in solvent placed in a non-solvent bath, for example water, which allows for solvent—non-solvent exchange and phase separation into polymer-rich and polymer-poor phases (Werber, Osuji and Elimelech, 2016). These two phases compose of the entire membrane where the polymer-rich phase makes up the polymer matrix and the polymer-poor phase makes up the pores in the membrane (Werber, Osuji and Elimelech, 2016).

Track etching is a process that can form ultrafiltration and microfiltration membranes (Werber, Osuji and Elimelech, 2016). The process occurs in two steps: 1) the bombardment of a track polymer with charged particles for partial degradation and 2) chemical etching to form pores of uniform size (Baker 2012) (Werber, Osuji and Elimelech, 2016). The main limitation for track etching is the low porosity so that pores do not overlap.

Thin-film composite polyamide membranes are the gold standard for nanofiltration, reverse osmosis and forward osmosis applications (Elimelech and Philip 2011) (Werber, Osuji and Elimelech, 2016). These membranes consist of a polysulfone support layer and a polyamide active layer. The process to create the polyamide active layer requires: first, that an aqueous diamine solution be brought into contact with a polysulfone support and second, that the support is immersed in an organic solvent phase containing TMC (Werber, Osuji and Elimelech, 2016). This process of polyamide formation is referred to interfacial polymerization, a complex process involving the condensation reaction of an amine and an acid chloride at the interface of an aqueous organic solution (Khorshidi, et al. 2016).

2.2 Desalination by Membrane-Based Reverse Osmosis

The need for reverse osmosis membranes is driven by the need for clean, accessible, drinking water for life. In the modern era, human activities pose threats to groundwater quality by contamination and overexploitation (Pangarkar, Sane and Guddad 2011). Aside from human activity, human population levels are rising thereby increasingly, stressing the current freshwater reserves (Li and Tian 2009). Statistically, less than 1% of the current water on Earth is freshwater available for humans to drink (Greenlee, et al. 2009). On the other hand, seawater makes up approximately 75% of the Earth's surface. In a time where stresses perpetuate on freshwater sources, outsourcing to seawater desalination will be critical. Reverse osmosis has the greatest potential, in terms of desalination technology, to treat seawater effectively, inexpensively, and with long-lasting integrity (Fritzmann, et al. 2007).

Reverse osmosis membranes are the most effective technology for removing salt from water because the lower energy requirements which is backed by nearly 100% removal (Pangarkar, Sane and Guddad 2011). These membranes outperform an alternative approach of thermal desalination by requiring less energy. Although the water is not evaporated then condensed, the water is under high pressure to cause a reverse osmotic effect which has a significant energy input.

Osmosis is the process by which two volumes of water with different salt concentrations, separated by an ion-impermeable membrane, will give rise to the collection of water in the volume of water with the greater salt concentration. An osmotic pressure is the driving force for water to reach this concentration equilibrium. As a result, an equal but

opposite pressure head accumulates in the saltier water. In this lab scale setup, the ion-impermeable membrane prevents the transport of salt to the less salty water.

In industry, engineers have developed reverse osmosis to take advantage of this natural phenomenon in salty waters. To overcome the osmotic pressure, engineers apply a pressure to push salt-free water through an impermeable TFC membrane meanwhile concentrating salt in the reject stream.

The fluxes of both salt and water are described in equations 2.1 and 2.2, respectively (Lind, et al. 2010). In order for water to flow to the less salty water, a hydraulic pressure is applied to overcome the resisting osmotic pressure for water to flow to the saltier water. Equally important, the flow of salt is determined by the change in concentration of feed and permeate. A and B are the water and salt permeability coefficients, respectively.

$$J_W = A(\Delta P - \Delta\pi) \quad \text{Eqn. 2. 1}$$
Water flux as a function of osmotic and applied pressure

$$J_S = B\left(C_f - C_p\right) = B\Delta C \quad \text{Eqn. 2. 2}$$
Salt flux as a function of concentration gradient from feed to permeate

Through empirical testing, J_w and J_s can be determined and A and B can be determined. Literature often utilizes these permeability coefficients to compare and contrast amongst membrane design. For A, an osmotic pressure must be qualitatively described and calculated for. Equation 2.3 models the assumptions adopted from research (Lind, et al. 2010).

$$\Delta\pi = 2RT(C_m - C_p) \quad \text{Eqn. 2. 3}$$
Osmotic pressure derived from pressure differences between the membrane and the permeate converted to concentrations using the ideal gas law

Finally, A can be calculated by empirically finding J_w and ΔP, rearranging equation 2-1 and supplementing equation 2.3 for the osmotic pressure, $\Delta\pi$. Similarly, B can be

calculated by empirically finding J_s, C_f, and C_p and rearranging equation 2.2. Models for A and B are demonstrated in equations 2.4 and 2.5, respectively.

$$A = \frac{J_w}{\Delta P - 2RT(C_m - C_p)} \quad \text{Eqn. 2. 4}$$

Model of water permeability coefficient

$$B = J_w \frac{1 - R_s}{R_s} \quad \text{Eqn. 2. 5}$$

Model of salt permeability coefficient

2.3 Graphene Oxide Novelty and Desalination Potential

GO is a nanomaterial made of single-layer sp2 bonded carbon atoms with oxygen functional groups found as defects in the aromatic carbon structure (Dreyer, et al. 2010). GO has been a material of interest to many disciplines for its unique electrical, structural, thermal, and optical properties (Geim and Novoselov 2007) (Sun, et al. 2008) (Huang, et al. 2011) (Weiss, et al. 2012). Since the award of the Nobel Prize in physics to Geim and Novoselov in 2010, graphene and its derivatives such as GO are quickly becoming the most patented form of carbon nanomaterials (Zurutuza and Marinelli 2014).

GO has been highlighted in membrane design for its novel properties including: well-defined nanometer pores that exhibit low frictional water flow inside them as well as the ability to sieve water molecules from water solutes, and the well-defined plate-like structure to from nanochannels for water transport (Mi 2014) (Joshi, et al. 2014). Figure 2.2 illustrates the ordered molecular structure of GO. GO can be synthesized in large quantities at low cost by the chemical oxidation of graphite to graphite oxide and subsequent exfoliation into GO (Dreyer, et al. 2010). The oxidation of graphite introduces hydroxyl, carboxyl, epoxy, and carbonyl functional groups in the aromatic structure of graphene (Dreyer, et al. 2010).The first synthesis of graphite oxide was described by

Brodie in 1859 and used nitric acid and potassium perchlorate as oxidizing agents (Dreyer, et al. 2010).

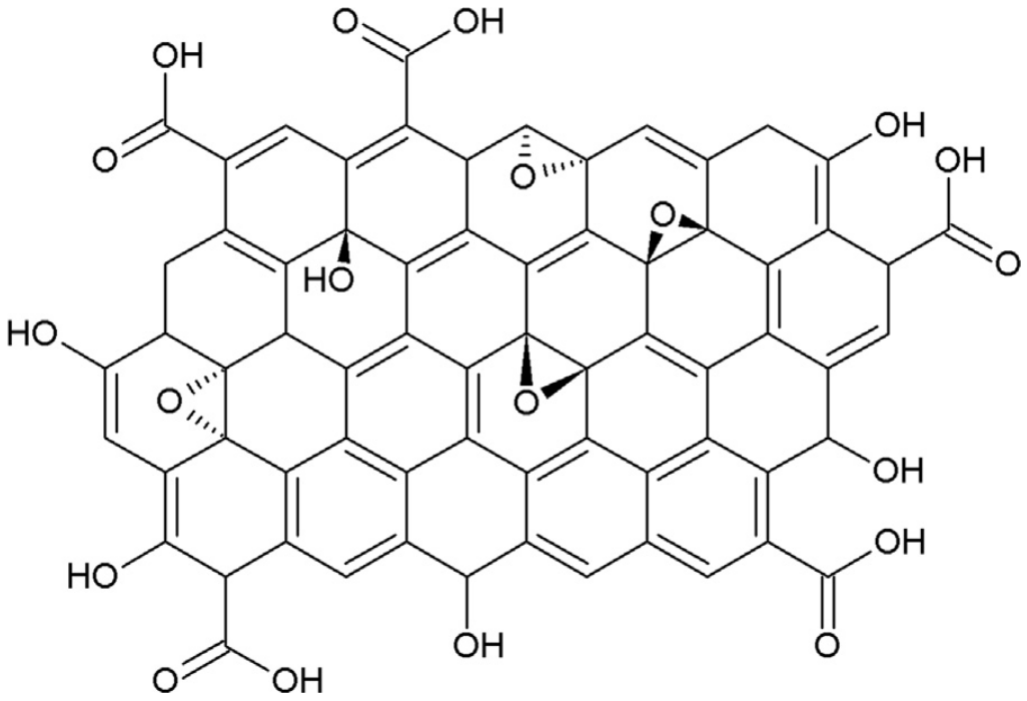

Figure 2. 2: Schematic image of GO molecular structure. Adopted from Chae (Chae, et al. 2015).

However, various oxidation protocols exist that produce different GO chemistries. Staudenmaier and Hofmann utilize concentrated sulfuric acid and nitric acid in combination with potassium chlorate. In comparison, Tung and Tour methods utilize potassium permanganate which produces a significantly more oxidized GO. Figure 2.3 illustrates the general process by which graphite can be oxidized to graphite oxide and sonicated to graphene oxide using specific oxidation protocols.

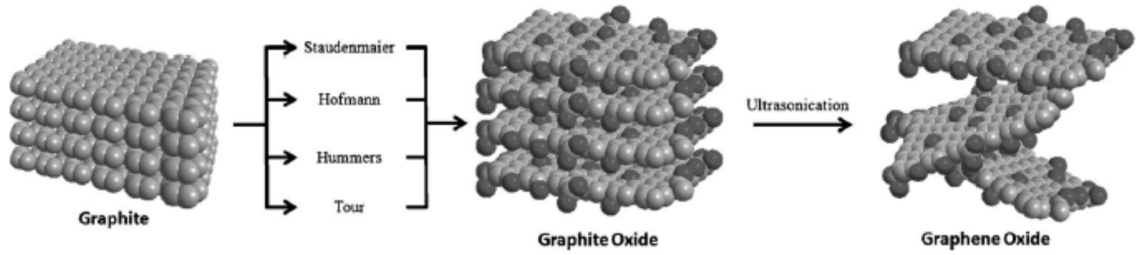

Figure 2. 3: Oxidation of graphite using different protocols. Adopted from Pumera (Pumera 2013).

Based on the oxygen content, electrostatic expulsion between graphene sheets forms varying interlayer spacing from 0.7-0.85nm (Dreyer, et al. 2010). Therefore, GO interlayer spacing is on the high end of the desalination range. By reducing GO from a highly-oxidized state, different interlayer spacing can be investigated inside the desalination range.

2.4 Nanomaterial-based Mixed Matrix Membranes for Desalination

MMMs have been studied using various types of nanomaterials for improved performance including: zeolites, carbon-nanotubes, or GO (Cay-Durgun, et al. 2017) (Werber, Osuji and Elimelech, Materials for next-generation desalination and water purification membranes 2016). MMM consist of an inorganic filler material inside a polymer matrix and have been studied for gas separation applications (Dong, Y. and Chen 2013) (Chung, et al. 2007). Recently, water separation membranes have been investigated to determine their enhancements using nanomaterials (Lau, et al. 2015). In these upcoming MMMs, GO has been investigated as an inorganic nanofiller (Yin, Zhu and Deng 2015) (Ali, et al. 2016) (Chae, et al. 2015) (Jeong, et al. 2007). These researchers have produced promising results in improving the performance of membrane technology without compromising its novel selectivity.

Recently, researchers embedded a modified hummers GO by dispersing the GO with TMC and Isopar-G solution used in interfacial polymerization (Yin, Zhu and Deng 2015). Others disperse the GO in the aqueous meta phenylenediamine (MPD) solution (Ali, et al. 2016) (Chae, et al. 2015) (Lee, et al. 2016). Research suggests that the GO should not be dispersed in the MPD solution because the GO may block pores of the polysulfone supporting material (Chan, Marand and Martin 2016). GO embedded MMMs have produced membranes with high permeability as well as salt permeability (Ali, et al. 2016). By reducing the GO, it may be possible to see the positive effects of GO permeability while not compromising salt rejection. Figure 2.4 illustrates the random embedment of GO in the thin-film layer of polyamide (Yin, Zhu and Deng 2015). The red arrows illustrate the water nanochannels that will act as molecular sieves for water to pass through and not water solutes. By reducing the GO, the spacing between these graphene sheets should be reduced. This tunable feature may lead to advances in reverse osmosis water treatment processes.

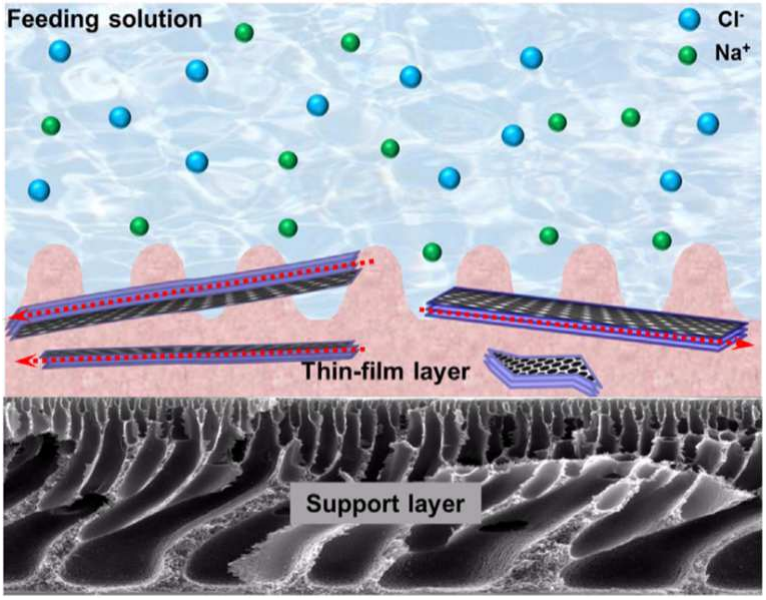

Figure 2. 4: Illustration of MMM with GO embedded in the thin-film layer of polyamide. Adopted from Yin (Yin, Zhu and Deng 2015).

Unlike GO, carbon nanotubes and 0D buckyballs do not consist of a plate-like structure (Geim and Novoselov 2007). As shown on Figure 2.4, single sheets of graphene are ideal for creating nanochannels in the polyamide layer of TFC membranes. During embedment of GO, the arrangement of the plates will be completely random. Therefore, the plates of GO may not act as channels from one side of the polyamide to the other but more as a web of passages available for water transport. In either case, the alteration of molecular transport from diffusion to size-exclusion should enhance permeability overall. Additionally, the web-like structure of GO will also provide added protection to polyamide in the event of chlorine or biofouling exposure.

Different GO chemistries, structures, and morphologies can exist due to their different synthesizing protocols. Individually, graphene sheet-spacing's fall in the range of 0.65-0.85nm. For molecular size-exclusion of individual molecules of water, or desalination range, the size exists from 3.4-7 angstroms (Werber, Osuji and Elimelech,

2016). As mentioned before, the reduced species of GO will possess smaller sheet spacing which is well within the desalination range. Figure 2.5 illustrates the changes in GO molecular structure from room temperature. 100ºC, 220ºC, and 500ºC (Pei and Cheng 2012). As the reducing temperature increases, the carbon and oxygen atoms entered an excited state and are capable of occupying leaving the structure as a gas or, in the case of carbon, occupying interstitial sites (Pei and Cheng 2012). Both phenomena support the conclusion that a reduced GO will have smaller pore sizes for molecular water sieving.

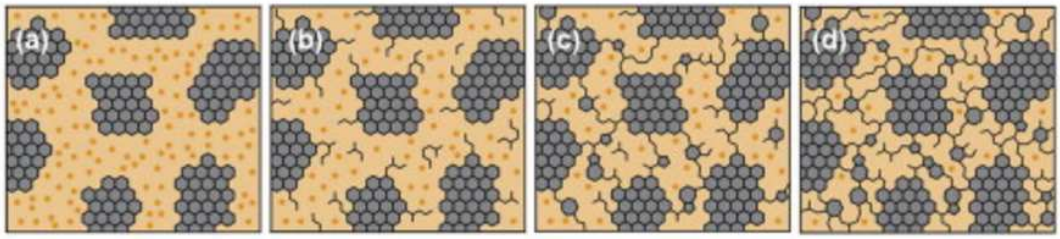

Figure 2. 5: Illustration of the changes in GO (gray) in molecular strucutre from (a) room temperature, (b) 100ºC, (c) 220ºC, and (d) 500ºC. The yellow color is unoccupied lattice space.

CHAPTER 3

METHODOLOGY

3.1 Graphene Oxide Synthesis

To generate GO materials of different oxidation level, different oxidation protocols were used. Bay Carbon graphite was oxidized using the four following protocols: Staudenmaier, Hoffmann, Tour, and Tung. Each method was adopted from Pumera et al. to form the GO used in this study (Pumera 2013). Additionally, Mercapto reduced GO was provided by the Seo lab at ASU using Kiwan Jeon's dissertation for synthesis (Jeon 2013).

3.1.1 Staudenmaier GO synthesis:

For the synthesis of GO by the Staudenmaier method,17.5mL of concentrated sulfuric acid (98%) and 9mL of nitric acid (>90%) were combined in a bulb-flask with a magnetic stirrer (Staudenmaier 1898). The mixture was cooled to 0^{o}C for 15 minutes. Then, 1g of graphite was added to the mixture under vigorous stirring to prevent agglomeration. Over a 15 minute interval, 11g of potassium chlorate was added to the mixture at 0^{o}C. This reaction will synthesize GO from graphite by utilizing the oxidizing potential of potassium chloride with strong acids, sulfuric and nitric. The process should be slow as the reaction produces chloride dioxide gas which is explosive at high concentrations. After the potassium chlorate is completely dissolved, the bulb-flask was loosely capped to allow the evolution of gas, and the mixture was stirred for 96 hours at room temperature. Once complete, the mixture was poured into 1L of nanopure water, filtered, redispersed, and cleaned.

3.1.2 Hofmann GO synthesis:

The synthesis of GO by the Hofmann synthesis is similar to the Staudenmaier synthesis but employs a less concentrated nitric acid solution for a less aggressive reaction. For this synthesis, 17.5mL of concentrated sulfuric acid (98%) and 9mL of nitric acid (63%) were combined in a bulb-flask with a magnetic stirrer. The mixture was cooled to 0ºC for 15 minutes. Then, 1g of graphite (Bay Carbon) was added to the mixture under vigorous stirring to prevent agglomeration. Over a 15 minute interval, 11g of potassium chlorate was added to the mixture at 0ºC. Again, this process will form GO from graphite by utililizing the oxidant potassium chloride with strong acids, sulfuric and nitric.The process should be slow as the reaction produces chloride dioxide gas which is explosive at high concentrations. After the potassium chlorate is completely dissolved, the bulb-flask was loosely capped to allow the evolution of gas, and the mixture was stirred for 96 hours at room temperature. Once complete, the mixture was poured into 1L of nanopure water, filtered, redispersed, and cleaned.

3.1.3 Tour GO synthesis:

The synthesis of GO by the Tour method employs sulfuric acid and potassium permanganate as the oxidizing agent. For this synthesis, a 9:1 mixture of concentrated (98%) H_2SO_4/H_3PO_4 (120:13.3mL) was made and 1g of graphite oxide flakes were added (Marcano, et al. 2010). The solution was bath sonicated under the chemical hood for 5 minutes to completely disperse the graphite in the mixture. Slowly, 6 grams of potassium permanganate were added to the mixture. The color of the mixture turned dark green due to the formation of MnO_7. MnO_7 is the highly oxidizing species responsible for the conversion of graphite to GO in the improved hummers method. The mixture was placed

into an ice bath to prevent the temperature from exceeding 50°C. Once complete, the reaction was heated reto 50°C and stirred for 12 hours. Then, the reaction was cooled to room temperature and poured into 400mL DI water ice. Finally, 3mL of hydrogen peroxide (30%?) were added to the mixture to quench the remaining MnO_4^- species to MnO_2. The reaction color turns bright yellow in this step. The mixture was allowed to rest overnight and was collected the next day.

3.1.4 Tung GO synthesis:

The Tung GO synthesis employs concentrated sulfuric acid and potassium permanganate as the oxidizing agent. Before the synthesis, the graphite underwent a pre-oxidation step to increase the effectivity of the oxidation. First, one gram of $K_2S_2O_8$ and one gram of P_2O_5 were placed into suspension with 5mL of concentrated sulfuric acid (98%) and mixed for 30 minutes. Then the graphite was added to the suspension. The mixture was allowed to mix for 4.5 hours and the temperature from was prevented from exceeding 80°C. The reaction utilizes $K_2S_2O_8$ and P_2O_5 as oxidizing agents to create GO from graphite. Once complete, the pre-oxidized graphite mixture was placed into 160mL of DI water and left to rest overnight. The next day, the mixture was vacuum filtered using a hydrophilic PTFE membrane (0.54 um) and washed with DI water to remove excess acid and reactants. The black solid was transferred to a petri dish and left to dry overnight at room temperature.

For the oxidation of GO, 3 grams of dried pre-oxidized graphite were placed into 120 milliliters of concentrated sulfuric acid. Slowly, 15 grams of potassium permanganate were added to the mixture. During this step, the mixture was placed in an ice bath to prevent the temperature from exceeding 10°C. Once complete, the reaction was allowed to occur

at 35ºC for 2.5 hours. Then, 231 mL of DI water were carefully added to the mixture to ensure the temperature did not exceed 50^{O}C. When complete, graphite suspension was allowed to react for 2 hours at room temperature. After, the solution was transferred to 720mL of DI water and 12.6mL of hydrogen peroxide (30%) and the color should turn to bright yellow.

3.1.5 Mercapto reduced GO synthesis:

The Mercapto reduced graphene oxide (MRGO) was produced by Haojie Zhang by following Kiwan Jeon's dissertation from ASU's SEMTE program (Jeon 2013). GO was produced by a modified hummers technique similar to the Tung synthesis. For the reduction of GO, about 0.2g of GO dispersed in deionized water (0.1wt%) was mixed with 130 mL of 1M NaOH aqueous solution. The solution was centrifuged and the supernatant was decanted. 0.0900g of amporphous boron powder (Alfa Aesar, 99.99%, 325 mesh) and 100 mL of deionized water were added to the precipitate and the mixture was sonicated until it became homogenous by viual inspection, The mixture was tehn dried in an oven at 110ºC overnight. 0.5347 g of sulfur powder (Alfa Aesar, 99.999%) was mixed with the dried precipitate and the mixture was subsequently placed in a fused silica tube (11 mm I.D.). The silica tube was then placed in a vacuum under 10^{-6} torr. The mixture was gradually heated at 100ºC/hr to 500ºC, held there for 10 hrs, and radiatively cooled to room temperature. The heat-reduced product was taken out, grounded, and sonicated in carbon disulfide to wash off the unreacted sulfur. Then the product underwent centrifugation and decantation and then allowed to dry in air. The product was then repeatedly washed with degassed hot water (~80ºC) until the supernatant became colorless in order to remove the unreacted boron sulfide and the byproduct B_2O_3. Next, 2 mL of 12 wt% sodium

borohydride ($NaBH_4$) in 14 M NaOH solution was added to the product and then the mixture was sonicated again for 10 minutes. A green color overcame the solution indicating the presence of polysulfide liberated from the product. Again, this process was repeated until the supernatant became colorless. 1 M HCl solution was added to give the final pH of about 1. The solution was centrifuged and decanted. The precipitate was rinsed multiple times with deionized water and subsequently washed with N,N-Dimethylformamide (DMF) and sonicated for 40 minutes in DMF. After centrifugation at 10,000 rpm for 10 minutes, the supernatant was collected to obtain dispersion.

3.2 Graphene Oxide Characterization

The different GO materials synthesized were characterized by Raman spectroscopy to confirm the oxidation of graphite to graphite oxide. A film of GO was formed by evaporating a solution of GO (1 mg/mL) on a clean glass slide. The Raman spectrum was measured on a Micro-Raman spectrometer (Leroy Erying Center for Solid State Science, ASU) using a 532 nm excitation. Raman spectroscopy identifies the change in molecular structure by analyzing peak shifts. In the case of graphene and GO, the D and G bands are likely to shift after oxidation. The peaks are listed alphabetically where the D-band exists around 1320 cm^{-1} and the G-band around 1570 cm^{-1} (de Faria, et al. 2015) (Baom, Zhang and Qi 2011) (Soldano, Mahmood and Dujardin 2010). An increase in the D/G ratio indicate the change in structure from graphite to graphite oxide.

The relationship between the oxygen content and the interlayer spacing in the different GO materials was established by x-ray diffraction (XRD) and x-ray photoelectron spectroscopy (XPS). XRD uses filtered x-rays generated by a cathode ray tube to emit monochromatic radiation, directed at a sample of graphene oxide of known angle of

incidence, to collect constructive interference from diffracted rays (Chipera and Bish 2013). By utilizing the angle of incidence, Bragg's law determines the interlayer spacing (d) between graphene plates in a graphene oxide. XRD was utilized to determine the sheet-spacing for all GOs and MRGO.

$n\lambda = 2dsin(\theta)$……*Eqn 3. 1 Bragg's law for crystal lattice spacing*

XPS measures the elemental composition, empirical formula, chemical state, and electronic state of the elements that exist within GO. These measurements are collected by irradiating GO with a beam of x-rays while simultaneously measuring the kinetic energy and number of electrons that escape from the surface of the GO (Vickerman 1997). The system requires a high vacuum of less than 10^{-8} mbar. XPS was used in this study to compare carbon to oxygen ratios of each sample.

The morphology of the GO materials produced was characterized by atomic force microscopy (AFM) and scanning electron microscope (SEM). AFM is a surface characterization tool that can provide an accurate measurement of the thickness of GO by tapping the surface of the GO with a silicon tip and recording the change in the distance of each tap as it travels across the GO surface. AFM utilizes changes in reflection of a laser that is reflected on a gold coating on the backside of the tip to detect thickness variation and this is recorded on a photodetector (Vickerman 1997). AFM produces a shade-scaled image based on height variations in the surface being analyzed. Thus, a clear image of GO platelets can be found and a thickness distribution can be recorded using AFM software analysis. The goal of AFM is to determine graphene sheet thickness as well as determine is the graphene oxide sheets are stacked or single 1D-material.

SEM works by scanning a focused electron beam over a surface to create an image. The electrons in the beam interact with the GO which produces excites electrons on the surface of the GO. These excited electrons are interpreted as signals than can be used to obtain information about the surface morphology and composition of the GO (Vickerman 1997). In this study, SEM was utilized to determine the surface morphology of STGO and MRGO.

3.3 TFC and TFC embedded with GO and MRGO Membrane Casting

The selected GO materials were integrated into TFC membranes during the interfacial polymerization step of membrane fabrication. Figure 3.1 illustrates the steps taken in membrane casting.

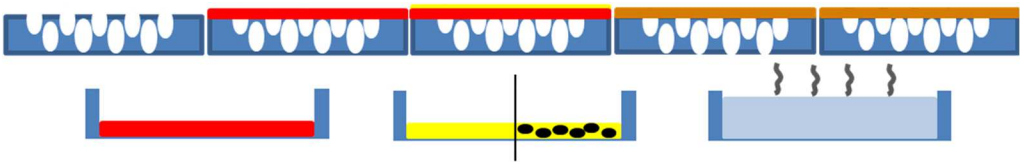

Figure 3. 1:Illustration of the formation of polyamide with and without GO. MPD in red, TMC in yellow, GO dispersed in TMC in black and yellow, polyamide in brown

To prepare the polyamide thin-film membrane, first the support layer of the membrane was cut to fit on a 9" x 5" glass plate. The dimensions used for the support material should be approximately 8 ¾" x 4 ¾". Then, three sprays of ethanol were applied and after that washed with milliQ water for 10 seconds. The support membrane was then placed into 1L of milliQ water. The membrane were allowed to sit for 1 day to remove any contaminants that may have adhered to the surface of the membrane by dissociating in the milliQ water.

The next day, the TMC (Sigma Aldrich) and MPD (Spectrum Chemicals) solutions were prepared. The TMC solution is approximately 0.15wt% TMC in Isopar-G.

Approximately, 150mL of this solution is used per cast. The MPD solution is 3.5wt% MPD in milliQ water.. Each solution was stirred for 4 hours at about 350 rpm.

The two post-treatment solutions were prepared. 1g of sodium bisulfite is added to 1L of milliQ water, and by adding, 1.5mL of sodium hypochlorite to 1L of milliQ water. The post-treatment solutions were stirred for at least 15 minutes at 350rpm.

A hot water bath was also prepared prior to casting by placing simmering-hot water in a Pyrex dish and on a hot plate. To perform the interfacial polymerization, the support membrane was taped to the 9" x 5" glass plate with chemical resistant tape. 10 minutes were allotted for taping between the membranes removal from the bottle and the immersion into the MPD solution. The support layer was secured to the glass plate so that only the active layer may be exposed to the solutions. Then, 150mL of MPD solutions were poured into a Pyrex dish on a 20 degree incline. The membrane taped to the glass plate was carefully placed into the MPD and Pyrex dish. 2 minutes were allowed for the MPD to diffuse into the polysulfone support layer. The MPD solution was replaced after every use. After 2 minutes, the membrane was removed and an air knife was used to remove excess droplets of MPD from the membrane surface.

The edges of the glass plate were dried and the glass plate and membrane were placed carefully into 150 mL of TMC solution and allowed to react for 1 minute. During this step, the MPD in the membrane will diffuse out of the membrane and corss-link with TMC at the water/solvent interface to precipitate as polyamide on the membrane. After, the glass plate was removed from membrane brick and allowed to sit for 2 minutes.

The glass plate was then placed into another Pyrex dish filled with simmering hot water (~95^{o}C) with the active side up. The membrane sat in the hot water for 2 minutes. It is important no boiling or bubbles arise as this will damage the polyamide structure.

After, the glass plate was removed from the hot water and the tape was removed from the plate. The membrane was transferred to the first post-treatment solution, sodium hypochlorite, without touching the active layer and allowed to sit for 2 minutes. This step permeabilizes the active layer, by removing excess MPD, to increase the permeability of the membrane. After, the membrane was transferred to the sodium bisulfite solution for 30 seconds to neutralize the hypochlorite solution and stop the permeabilization process. During this process, the simmering hot water should be replaced. Then, the membrane was carefully placed active side down in the hot water bath for 2 minutes.

Finally, the membrane was removed from hot water bath and placed to store in a container filled with milliQ water. Again, the hot water should be replaced before the next casting. This casting protocol should be repeated for each prepped membrane support layer intended for casting.

3.4 Casted MMM and TFC RO Performance Testing

The membranes were loaded into six stainless steel cells in a lab-scale reverse osmosis system. The system maintained an operating temperature of 20^{o}C and variable humidity ranging from 30-50%. After each loading, old oil from the pump would be replaced with fresh, new oil to ensure consistent operating performance.

A total of 6 membranes were tested in total: 2 control TFC, 2 STGO, and 2 MRGO. The membrane tests took approximately two days to complete. The first 24 hours are dedicated for membrane compaction at a pressure of 300 psi. After smooth operating

performance at 300 psi for 24 hours, the pure water flow rate is tested and then the system is spiked with 56 grams of salt into 28 L of milliQ water. After another 2 hours, the salt water flow rate is tested and the permeate of each cell is collected as well as the feed to determine conductivities. Each test determined pure water flux, salt water flux, and permeate and feed conductivity. The testing produced permeability and salt coefficients for each membrane and these are used to compare the performance of each membrane.

Equation 3.2 models pure water flux by measuring the flowrate across the membrane with milliQ water. The flow rate is found using a flow meter device. The volumetric flow rate is then divided by the area of the membrane to calculate for the pure water flux (PWF). Ultimately, this data would allow for the calculation of water permeability coefficient (A). The water and salt permeability coefficients calculations were demonstrated earlier.

$$PWF = \frac{Volumetric\ Flow\ Rate}{Crossflow\ Area} \quad \text{.....Eqn 3. 2}$$

Pure Water Flux (PWF) as a function of volumetric flowrate and cross-flow area

Similarly, the salt water flux is determined by measuring the flowrate across the membrane with 2g/L of salt in milliQ water. Again, the volumetric flow rate is then divided by the area of the membrane to calculate the salt water flux (SWF). Ultimately, this data would allow for the calculation of salt permeability coefficient.

$$SWF = \frac{Volumetric\ Flow\ Rate}{Crossflow\ Area} \quad \text{.....Eqn 3. 3}$$

Salt Water Flux (SWF) as a function of volumetric flowrate and cross-flow area

Permeate (P) and feed (F) conductivity are taken after running the system for 2 hours with salt added. Ultimately, this data would allow for the calculations of salt rejection

(equation 3.4), water permeability coefficient (equation 2.4), and the salt permeability coefficient (equation2.5).

$$R_s * 100 = Selectivity = \left(1 - \frac{P}{F}\right) * 100 \ldots\ldots\ldots\ldots\ldots\ldots\ldots\ldots\ldots\ldots\ldots\ldots\ldots\ldots Eqn\ 3.\ 4$$

Selectivity or salt rejection of a membrane based on conductivities of feed and permeate solutions

CHAPTER 4

RESULTS AND DISCUSSION

4.1 Graphene Oxide Characterization

The XRD spectra of the starting graphite and synthesized GO are provided below in Figure 4.1. Each peak corresponds to a unique 2θ value depending on the specific crystallography of each GO analyzed. These peaks arise from different d-spacing, or the spacing between the graphene sheets. The oxidation of graphite to GO increase the d-spacing from 3.2 angstrom for graphite to 6.47, 7.03, 7.77, and 8.34 angstrom for the GO produced by the Staudenmaier. Hofmann, Tour, and Tung synthesis, respectively. In comparison, a post-oxidation treatment to reduce GO, the MRGO, reduced the d-spacing to 3.8 angstrom.

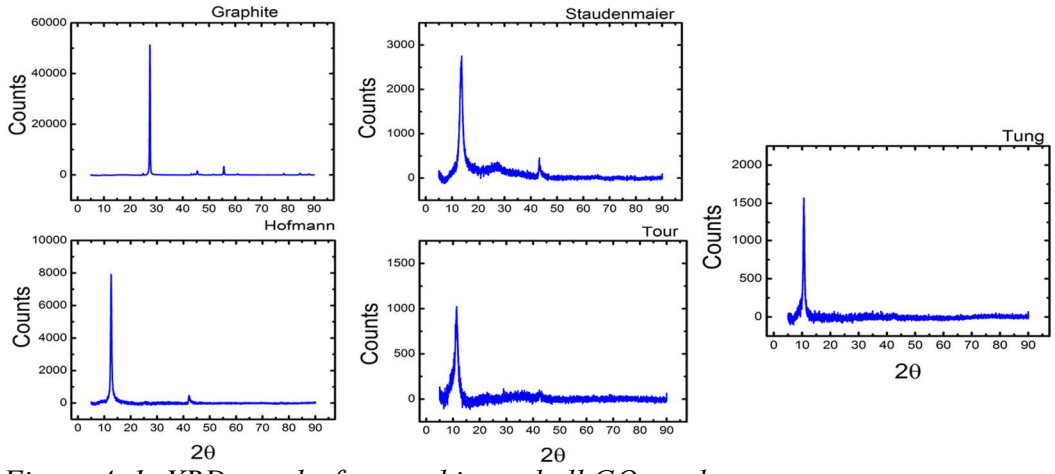

Figure 4. 1: XRD graphs for graphite and all GO syntheses.

The decrease in d-spacing after reduction indicates that changes in the oxygen content influence the interlayer distance between the sheets (Moon, et al. 2010). To verify this relationship existed in the different GO materials synthesized, XPS analyses were performed to determine the oxygen content for each of the GO and graphite. The results

are listed in Table 4.1 The data shows the trend that as interlayer spacing decreases, the corresponding 2θ values increases.

Table 4. 1: Corresponding graphene sheet spacing, 2θ values, and carbon to oxygen ratios for each GO.

Graphene Oxide	2θ (degrees)	d-spacing (Angstroms)	C:O ratio
Staudenmaier	13.68	6.47	4
Hofmann	12.58	7.03	3
Tour	11.40	7.77	1.79
Tung	10.06	8.34	1.93
MRGO	25.6*	3.8	15
Graphite	27.52	3.2	61

*The MRGO is estimated because it is a 1-dimensional material and therefore does not possess as clear XRD spike as other GO.

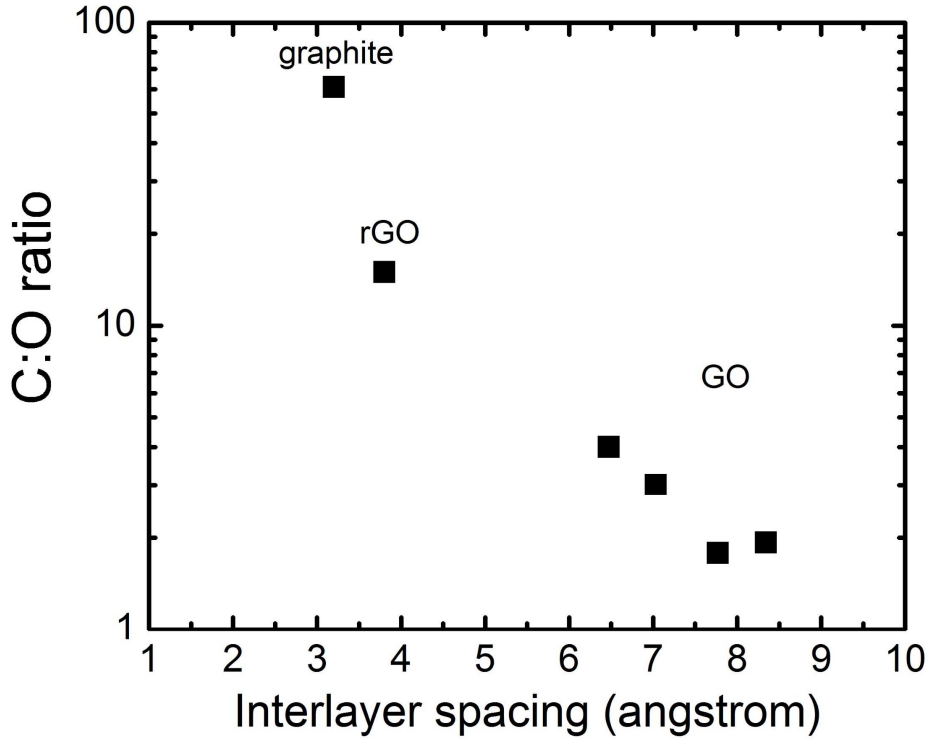

Figure 4. 2: C:O ratio as a function of interlayer spacing for GO, rGO, and graphite.

Figure 4.2 combines data from XPS and XRD to illustrate the relationship of C:O ratio and of d-spacing by plotting. As anticipated, as the oxygen content of a graphene

species increased, the interlayer graphene sheet spacing increased as well. This is attributable to the increased electrostatic repulsion provided by the negatively charged oxygen functional groups.

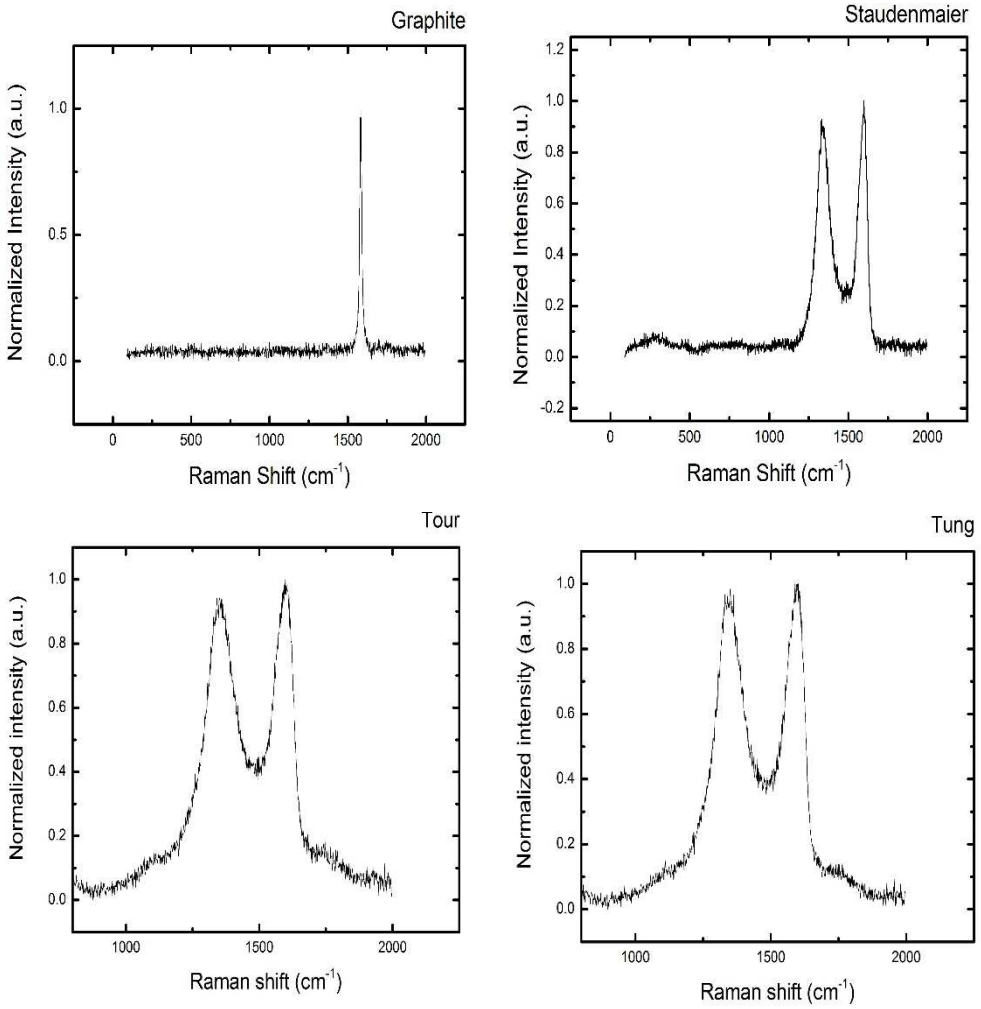

Figure 4. 3: Raman spectroscopy for Staudenmaier, Tour and Tung graphene oxides as well as the starting graphite.

Figure 4.3 illustrates the Raman spectroscopy images for Staudenmaier, Tour, and Tung GOs as well as the starting graphite material. Each GO has both the D and G peaks associated with graphene materials. The D band is caused by the disordered structure of graphene that emerges after the oxidation of graphene. As shown in Figure 4.2, the starting

graphite does not contain a D band because the order has not been dismantled by oxygen functional groups in the lattice. The G band arises from the stretching of the C-C bond in graphitic materials. Therefore, comparing the D and G band can provide insight regarding the disordered nature of the sample. The more oxidized samples of Tour and Tung have higher D to G ratios which is confirmed through Table 4.2. Compared to the starting graphite, there is a clear shift in peaks due to the emergence of a D-peak in the graphene oxides. This confirms the oxidation of graphite to a less ordered graphene oxygen as well as confirms the hypothesis regarding XRD and XPS oxidation trends.

Table 4. 2:Raman spectroscopy D to G intensity ratio for Graphite, Staudenmaier GO, Tour GO, and Tung GO.

Material	D to G Ratio
Graphite	0
Staudenmaier	0.920
Tour	0.939
Tung	0.983

4.2 Material Selection for Membrane Fabrication

As a result of the data from XRD, XPS, and Raman, Staudenmaier GO was selected for further MMM testing as it possessed a more promising interlayer spacing of 6.47 angstroms, well within the desalination range compared to its counterparts. Similarly, MRGO was also used for its significantly lower d-spacing range of 3.8 angstroms.

4.3 Morphological Characterization of GO

Figure 4.4 illustrates SEM images of MRGO, adopted from Kiwan Jeon (Jeon 2013). Single graphene sheets can be found at 2 different magnifications. Qualitatively, the image displays a fairly uniform MRGO sheets.

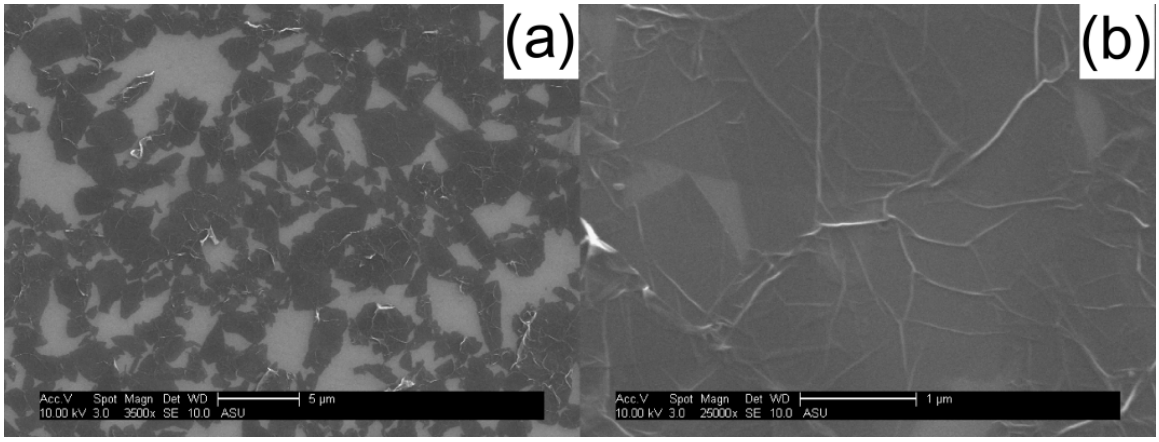

Figure 4. 4: SEM of MRGO. Adopted from Kiwan Jeon's dissertation (Jeon, 2013).

Figure 4.5 illustrates an SEM image of Staudenmaier GO. The image reveals a stacked layer of graphene sheets instead of uniform single sheets.

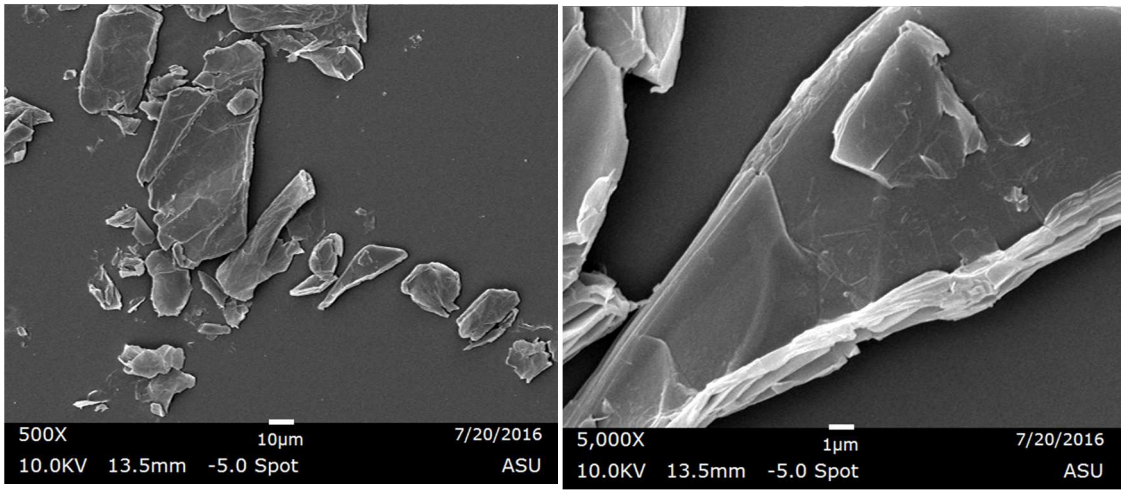

Figure 4. 5: SEM images of Staudenmaier GO.

Figure 4.6 illustrates AFM measurements of MRGO to determine graphene sheet thickness of approximately 1.4nm, adopted from Kiwan Joen's Dissertation (Jeon 2013).

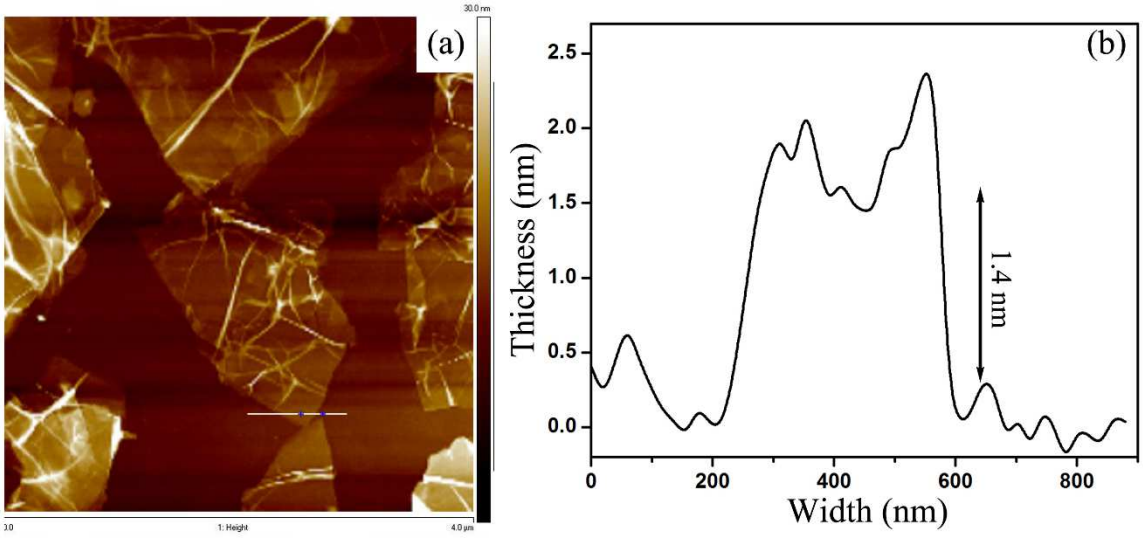

Figure 4. 6: (a) AFM and (b) thickness analysis of MRGO. Adopted from Kiwan Jeon Dissertation (Jeon, 2013).

Figure 4.7 illustrates AFM measurements of STGO to determine graphene sheet thickness of approximately 1.5nm.

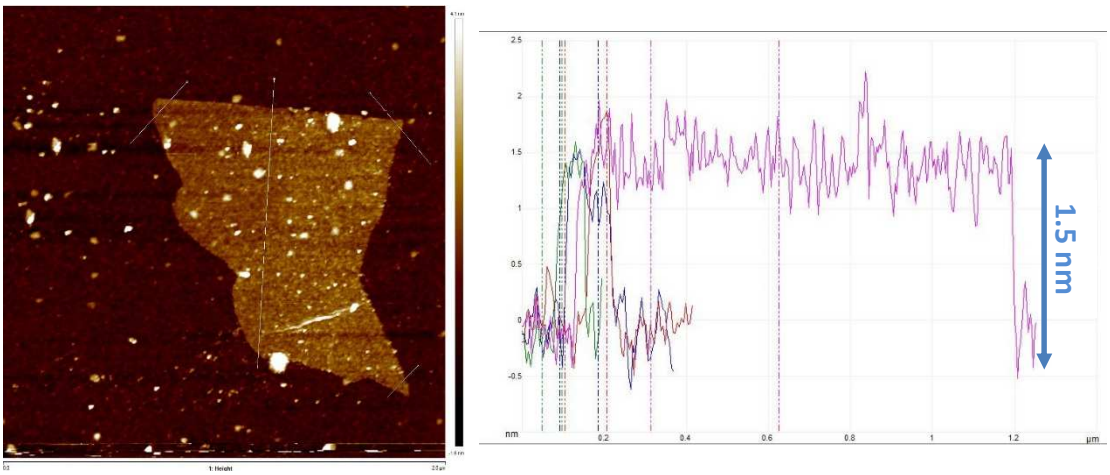

Figure 4. 7: AFM image of Staudenmaier GO. 4 Intersecting slices chosen to quantify the thickness.

For MMMs, RGO possesses the ideal graphene sheet spacing for molecular sieving as well as lacks the reactive carboxyl groups when dispersed in TMC and Isopar-G solution (Jeon 2013). Additionally, RGO does not disperse well in water solutions as it is hydrophobic, therefore, it is favorable to disperse in a solvent like Isopar-G.

Research identified that the chloride in TMC would react with the carboxyl groups in GO but this reaction is slower than the interfacial polymerization reaction (Yin, Zhu and Deng 2015). Therefore, when casting GO in TMC, the dispersion should be used for interfacial polymerization shortly after combining the two.

4.4 Morphological Characterization of GO, MRGO, and TFC Membranes

The membranes were characterized using SEM to identify the morphology changes between MMMs and TFC membranes. Figure 4.8 illustrates the different morphologies observed between TFC, Staudenmaier GO MMM, and MRGO-MMM.

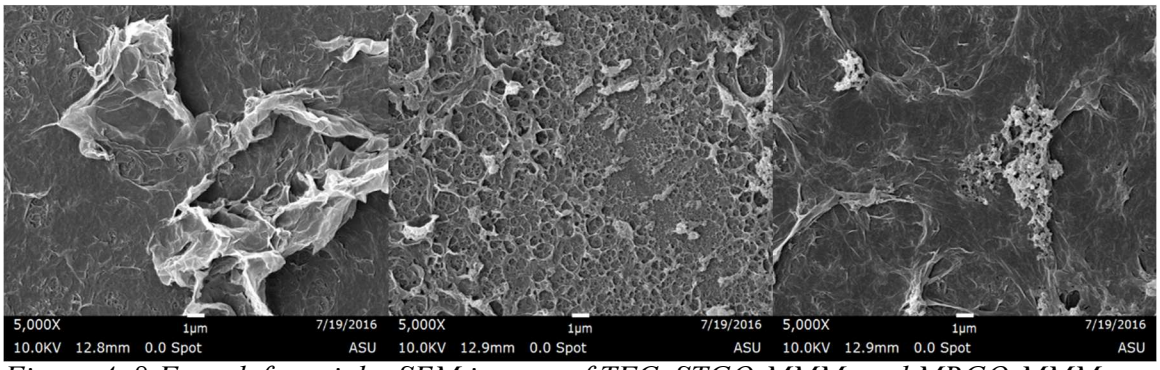

Figure 4. 8:From left to right, SEM images of TFC, STGO-MMM, and MRGO-MMM.

4.5 GO, MRGO, and TFC Membrane RO Performance

As illustrated in figure 4.9, the TFC membranes were outperformed by the MRGO membranes in water permeability, A. However, salt permeability, B, increased when GO and MRGO were added to the polyamide layer. The results require further testing as there is only two data points per membrane type. One data point from the MRGO section actually matched salt permeability coefficient of the optimal TFC membranes. Based on further testing, a stronger conclusion will be found regarding the B value for MMM embedded

with GO. These data were formulated from pure water flux, salt water flux, and selectivity as mentioned earlier.

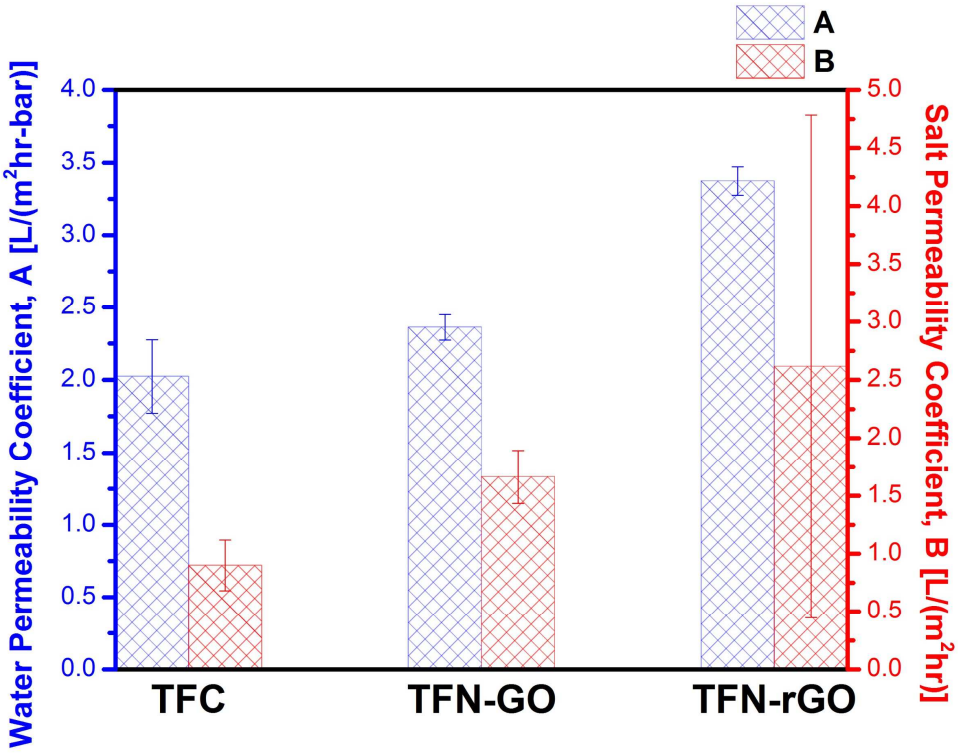

Figure 4. 9:Average water and salt permeability coefficients for 3 membranes: TFC, TFN-STGO, and TFN-MRGO.

CHAPTER 5

CONCLUSION

The positive results regarding membrane performance after embedding MRGO in the polyamide active layer should encourage future research. The GO membrane performed with increased permeability compared to the TFC membrane; however, the solute permeability also increased which is not ideal. Alternatively, the MRGO membrane performed with higher permeability than the GO membrane; but, also demonstrated a higher solute permeability than the GO membrane. The permeability-selectivity data illustrates that the MRGO membrane displayed a significant deviation for the solute permeability and should be further investigated to determine where the value precisely is. However, the GO membrane solute permeability displayed a more precise statistic than the MRGO. Therefore, the ability for GO/MRGO to improve permeability of TFC membranes is novel but further testing is required to determine if the error bar for the MRGO membrane solute permeability should be equivalent or less than the TFC membrane.

The spectrum of molecular size-exclusion of water was not fully investigated. There is room for exploration between the bounds of 0.4-0.6nm sheet spacing. It is possible MRGO is too exclusive and that a slightly larger pore size for water will produce even better results for the permeability coefficient to reach >6LMHbar^{-1}.

Also, the effects that different GOs created with different oxidation protocols have on their integrity in the polyamide matrix and their effect on performance should be investigated further. Different GOs will have different ratios of carbon to oxygen as well as different oxygen functional groups. Varied oxygen functional groups will cause graphene oxides to exhibit different levels of resilience within the polyamide matrix.

Finally, a key phenomenon not fully understood by many researchers is the degradation or resilience of these membranes. Measures should be taken to calculate graphene oxide, or any nanomaterial, that is removed from a membrane embedding during operation. Ultimately, to improve public perception, there must be evidence that research has taken into account the likelihood of graphene oxide removal during reverse osmosis operation and to what extent.

Things to consider regarding this research outside of the future work aspect include the fact that membrane support material is 1) hard to find and 2) hard to prepare polyamide active layers to match those of the industrial level. Thankfully, the Lind lab was able to provide and excellent support material along with the knowledge on how to process it to make a good support. However, our attempt to transfer the membrane fabrication method on a different support was met with a lot of challenges in reproducibility. Finding an equally superior support material to the initial material used was a struggle and will be an issue for future membrane development at the bench-scale.

Membrane technologies enable water treatment technologies far superior than older Victorian design. This study identifies that MMMs have a great potential, especially in the realm of GO and RGO. Research proves that both these materials have potential to revolutionize the membrane industry and spark insight for future materials. The ability of GO and RGO to break away from the permeability-selectivity curve and produce membranes of qualities incapable of polyamide alone speaks for itself. The need for clean, accessible, drinking water will continue to drive innovations in membrane, specifically reverse osmosis membrane, design and material innovation will continue to be highlighted in the coming years.

REFERENCES

Ali, Mohamed E.A., Leyi Wang, Xinyan Wang, and Xianshee Feng. 2016. "Thin film composite membranes embedded with graphene oxide for water desalination." *Desalination* 67-76.

Amadei, Carlo, and Chad Vecitis. 2016. "How to Increase the SIgnal-to-Noise Ratio of Graphene Oxide Membrane Research." *Journal of Physical Chemistry* 3791-3797.

Baker, R.W. 2012. "Membrane technology and applications." *John Wiley and Sons.*

Baom, Q., D. Zhang, and P. Qi. 2011. "Synthesis and Characterization of Silver Nanoparticles and Graphene Oxide Nanosheet Composites as a Bactericidal Agent for Water Disinfection." *Journal of Colloid Interface Science* 463-270.

Cay-Durgun, Pinar, Cailen McCloskey, John Konecny, Afsaneh Khosravi, and Mary Laura Lind. 2017. "Evaluation of thin film nanocomposite reverse osmosis membranes for long-term brackish water desalination performance." *Desalination* 304-312.

Chae, Hee-Ro, Jaewoo Lee, Chung-Hak Lee, In-Chul Kim, and Pyung-Kyu Park. 2015. "Graphene oxide-embedded thin-film composite reverse osmosis membrane with high flux, anti-biofouling, and chlorine resistance." *Journal of Membrane Science* 128-135.

Chan, Wai-Fong, Eva Marand, and Stephen M. Martin. 2016. "Novel xwitterion functionalized carbon nanotube nanocomposite membranes for improved RO performance and surface anti-biofouling resistance." *Journal of Membrane Science* 125-137.

Chipera, Steve J., and David L. Bish. 2013. "Fitting full X-ray diffraction patterns for quantitative analysis: a method quanitifying crystalline and disordered phases." *Advances in Materials Physics and Chemistry* 47-53.

Chung, T.S., L. Y. Jiang, Y. Li, and S. Kulprathipanja. 2007. "Mixed matrix membranes (MMMs) comprising organic polymers with dispersed inorganic fillers for gas separation." *Prog. Polym. Sci.* 483-507.

de Faria, Andreia F., Francois Perreault, Evyatar Shaulsky, Laura H. Aria Chavez, and Menachem Elimelech. 2015. "Antimicrobial electrospun biopolymer nanofiber

mats functionalized with graphene oxide - silver nanocompsites." *Applied Materials and Interfaces* 12751-12759.

Dong, G. X. L., H. Y., and V. K. Chen. 2013. "Challenges and opportunities for mixed-matrix membranes for gas separation." *Journal of Material Chemistry* 4610-4630.

Dreyer, Daniel R., Sungjin Park, Christopher W. Bielawski, and Rodney S. Ruoff. 2010. "The chemistry of graphene oxide." *Chem. Soc. Rev.* 228-240.

Elimelech, M. 2006. "The global challenges for adequate and safe water." *Journal for Water Supply Research* 3-10.

Elimelech, Menachem, and William A. Philip. 2011. "The Future of Seawater Desalination: Energy, Technology, and the Environment." *Science* 712-717.

Fritzmann, C., J. Lowenburg, T. Wintgens, and T. Melin. 2007. "State-of-the-art reverse osmosis desalination." *Desalination* 1-76.

Ganesh, B. M., Arun M. Isloor, and A. F. Ismail. 2013. "Enhanced hydrophilicity and salt rejection study of graphene oxide-polysulfone mixed matrix membrane." *Desalination* 199-207.

Geim, A.K., and K.S. Novoselov. 2007. "The rise of graphene." *Nature Materials* 183-191.

Geise, Geoffrey M., Ho Bum Park, Alyson C. Sagle, Benny D. Freeman, and James E. McGrath. 2011. "Water permeability and water/salt selectivity tradeoff in polymers for desalination." *Journal of Membrane Science* 130-138.

Goh, Kunli, Huseyin Karahan, Li Wei, Tae-Hyun Bae, Anthony Fane, Rong Wang, and Yuan Chen. 2016. "Carbon Nanomaterials for Advancing Separation Membranes: A Strategic Perspective." *Carbon* 695-706.

Greenlee, L. F., D. F. Lawler, B. D. Freeman, B. Marrot, and P. Moulin. 2009. "Reverse osmosis desalination: water sources, technology, and today's challenges." *Water Research* 2317-2348.

Huang, Xiao, Zongyou Yin, Shixin Wu, Xiaoying Qi, Qiyuan He, Qichun Zhang, Qingyu Yan, Freddy Boey, and Hua Zhang. 2011. "Graphene-Based Materials: Synthesis, Characterization, Properties, and Applications." *Small* 1876-1902.

Ismail, A.F., P.S. Goh, S.M. Sanip, and M. Aziz. 2009. "Transport and separation properties of carbon nanotube-mixed matrix." *Separation and Purification Technology* 12-26.

Jeon, Kiwan. 2013. *Synthesis and Characterization of Thionated Reduced Graphene Oxides and Their Films.* Tempe: Arizona State University.

Jeong, Byeong-Heon, Eric M. V. Hoek, Yushan Yan, Arun Subramani, Xiaofei Huang, Gil Hurwitz, Asim K. Ghosh, and Anna Jawor. 2007. "Interfacial polymerization of thin film nanocomposites: A new concept for reverse osmosis membranes." *Journal of Membrane Science* 1-7.

Joshi, R.K., P. Carbone, F.C. Wang, V.G. Kravets, Y. Su, I.V. Grigorieva, HA.. Wu, A.K. Geim, and R.R. Nair. 2014. "Precise and ultrafast molecular sieving through graphene oxide membranes." *Science* 752-754.

Khorshidi, B., T. Thundat, B.A. Fleck, and M. Sadrzadeh. 2016. "A novel approach toward fabrication of high perfromance thin film composite polyamide membranes." *Science* 22069.

Kolphin, D.W. 2002. "Pharmaceuticals, hormones, and other organic wastewater contaminants in U.S. streams." *Environmental Science and Technology* 1202-1211.

Lau, W., S. Gray, T. Matsuura, D. Emadzadeh, J.P. Chen, and A. Ismail. 2015. "A review on polyamide thin film nanocomposite (TFN) membranes: history, applications, challenges, and apporaches." *Water Research* 306-324.

Lee, Byeongho, Kunzhou Li, Hong Sik Yoon, Jeyong Yoon, Yeongbong Mok, Yan Lee, Hong H. Lee, and Yong Hyup Kim. 2016. "Membrane of Functionalized Reduced Graphene Oxide nanoplates with Angstrom-Level Channels." *Scientific Reports* 6.

Li, Yajing, and Kunpeng Tian. 2009. "Application of vacuum membrane distallation in water treatment." *Journal of Sustainable Development* 183-186.

Lind, Mary L., Asim K. Ghosh, Anna Jawor, Xiaofei Huang, William Hou, Yang Yang, and Eric M. V. Hoek. 2009. "Influence of Zeolite Crystal Size on Zeolite-Polyamide Thin Film Nanocomposite Membranes." *Langmuir* 10139-10145.

Lind, Mary Laura, Daniel Eumine Suk, The-Vinh Nguyen, and Eric M. V. Hoek. 2010. "Tailoring the Structure of Thin FIlm Nanocomposite Membranes to Achieve Seawater RO Membrane Performance." *Environ. Sci. Technol.* 8230-8235.

Mahmoud, Khaled A., Bilal Mansoor, Ali Mansour, and Marwan Kharisheh. 2014. "Functional Graphene Nanosheets: The Next Generation Membranes for Water Desalination." *Desalination* 208-225.

Marcano, D.C., D.C. Kosynkin, J.M. Berlin, A. Sinitskii, Z. Sun, A. Slesarev, L.B. Alemany, W. Lu, and J.M. Tour. 2010. "Improved synthesis of graphene oxide." *ACS Nano* 4806-4814.

Mi, Baoxia. 2014. "Graphene Oxide Membranes for Ionic and Molecular Sieving." *Science* 740-742.

Misdan, N., W. J. Lau, and Ahmad Fauzi Ismail. 2011. "Seawater Reverse Osmosis desalination by thin-film composite membrane-Current development, challenges, and future prospects." *Desalination* 228-237.

Moon, In Kyun, Junghyun Lee, Rodney S. Ruoff, and Hyoyoung Lee. 2010. "Reduced graphene oxide by chemical graphitization." *Nature Communications* 1-6.

Moore, Emily. 2016. *Fourier Transform Infrared Spectroscopy (FTIR): Methods, Analysis and Research Insights.* Nova.

Pangarkar, Bhuasaheb L., Mukund G. Sane, and Mahendra Guddad. 2011. "Reverse Osmosis and Membrane Distallation for Desalination of Groundwater: A Review." *ISRN Materials Science* 9 pages.

Paul, D. R. 2004. "Reformulation of the solution-diffusion theory of reverse osmosis." *Journal of Membrane Science* 371-386.

Pei, Songfeng, and Hui-Ming Cheng. 2012. "The reduction of graphene oxide." *Carbon* 3210-3228.

Pendergast, MaryTheresa M., and Eric M.V. Hoek. 2011. "A review of water treatment membrane nanotechnologies." *Energy Environ. Sci.* 1946-1971.

Perreault, Francois, Andreia Fonseca de Faria, and Menachem Elimelech. 2015. "Envionmental applications of graphene-based nanomaterials." *Chemical Society Reviews* 5861-5896.

Perreault, Francois, Andreia Fonseca de Faria, and Menachem Elimelech. 2015. "Environmental Applications of Graphene-Based Nanomaterials." *Chem. Soc. Rev.* 5861-5896.

Perreault, Francois, Marissa E. Tousley, and Menachem Elimelech. 2014. "Thin-Film Composite Polyamide Membranes Functionalized with Biocidal Graphene Oxide Nanosheets." *Environmental Science and Technology* 71-76.

Pumera, Elaine Lay Khim Chng and Martin. 2013. "The Toxicity of Graphene Oxides: Dependence on the Oxidative Methods Used." *Chem. Eur. J.* 8227-8235.

Qu, Xiaolei, Pedro J. J. Alvarez, and Qilin Li. 2013. "Applications of nanotechnology in water and wastewater treatment." *Water Research* 3931-3946.

Schwarzenbach, R. P. 2006. "The challenge of micropollutants in aquatic systems." *Science* 1072-1077.

Semiat, Raphael. 2008. "Energy Issues in Desalination Processes." *Environ. Sci. Technol.* 8193-8201.

Shannon, M.A. 2008. "Science and technology for water purification in the coming decardes." *Nature* 301-310.

Soldano, C., A. Mahmood, and E. Dujardin. 2010. "Production, Properties, and Potential of Graphene Oxide." *Carbon* 2127-2150.

Staudenmaier, L. 1898. "Verfahren zur Darstellung der Graphitsäure." *European Journal of Inorganic Chemistry* 1481-1487.

Sun, Pengzham, Kunlin Wang, and Hongwei Zhu. 2016. "Recent Developments in Graphene-Based Membranes: Structure, Mass-Transport Mechanism and Potential Applications." *Advanced Materials* 2287-2310.

Sun, Xiaoming, Zhuang Liu, Kevin Welsher, Joshua Tucker Robinson, Andrew Goodwin, Sara Zaric, and Hongjie Dai. 2008. "Nano-graphene oxide for cellular imaging and drug delivery." *Nano Research* 8021-8028.

Tang, J.Y., F. Busetti, J.W. Charrois, and B.I. Escher. 2014. "Which chemicals drive biological effects in wastewater recycled water?" *Water Research* 289-299.

Tiraferri, Alberto, Yan Kang, Emmanuel P. Giannelis, and Menachem Elimlech. 2012. "Superhydrophilic Thin-Film Composite Forward Osmosis Membranes for Organic Fouling Control: Fouling Behavior and Antifouling Mechanisms." *Environ. Sci. Technol.* 11135-11144.

Vickerman, John C. 1997. "Surface Analysis-The Principal Techniques." *John Wiley and Sons.*

Weiss, Nathan O., Hailong Zhou, Lei Liao, Yuan Liu, Shan Jiang, Yu Huang, and Xiangfeng Duan. 2012. "Graphene: An Emergin Electronic Material." *Advanced Materials* 5782-5825.

Werber, Jay R., Akshay Deshmukh, and Menachem Elimelech. 2016. "The Critical Need for Increased Selectivity, Not Increased Permeability, for Desalination Membranes." *Environ. Sci. Technol.* 112-120.

Werber, Jay R., Chinedum O. Osuji, and Menachem Elimelech. 2016. "Materials for next-generation desalination and water purification membranes." *Nature Reviews Materials* 1.

Yin, Jun, Guocheng Zhu, and Baolin Deng. 2015. "Graphene Oxide enhanced polyamide thin-film nanocomposite membrane for water purification." *Desalination* 93-101.

Zodrow, Katherine, Lena Brunet, Shaily Mahendra, Dong Li, Anna Zhang, Qilin Li, and Pedro J.J. Alvarez. 2009. "Polysulfone ultrafiltration membranes impregnated with silver nanoparticles show improved biofouling resistance and virus removal." *Water Research* 715-723.

Zurutuza, Amaia, and Claudio Marinelli. 2014. "Challenges and opportunities in graphene commercialization." *Nature Nanotechnology* 730-734.

APPENDIX A

EQUATIONS

Equation Page

Eqn. 2. 1 10

Eqn. 2. 2 10

Eqn. 2. 3 10

Eqn. 2. 4 11

Eqn. 2. 5 11

Eqn 3. 1 22

Eqn 3. 2 26

Eqn 3. 3 26

Eqn 3. 4 27